Photonic Crystals Based on Periodic Arrays of Aligned Carbon Nanotubes

ARTICLE *in* NANO LETTERS · NOVEMBER 2002

Impact Factor: 13.59 · DOI: 10.1021/nl0258271

NANO LETTERS

2003
Vol. 3, No. 1
13−18

Photonic Crystals Based on Periodic Arrays of Aligned Carbon Nanotubes

K. Kempa,[†] B. Kimball,[‡] J. Rybczynski,[§] Z. P. Huang,[||] P. F. Wu,[⊥] D. Steeves,[‡] M. Sennett,[‡] M. Giersig,[§] D. V. G. L. N. Rao,[⊥] D. L. Carnahan,[||] D. Z. Wang,[†] J. Y. Lao,[†] W. Z. Li,[†] and Z. F. Ren*,[†]

Department of Physics, Boston College, Chestnut Hill, Massachusetts 02467, U.S. Army Soldier & Biological Chemical Command, Natick Soldier Center, Natick, Massachusetts 01760, Hahn-Meitner-Institute, D-14109, Berlin, Germany, NanoLab, Inc., Brighton, Massachusetts 02135, and University of Massachusetts, Boston, Massachusetts 02125

Received October 3, 2002; Revised Manuscript Received November 2, 2002

ABSTRACT

We demonstrate here that large area periodic arrays of well-aligned carbon nanotubes can be fabricated inexpensively on Ni dots made by the process of self-assembly nanosphere lithography. These periodic arrays appear colorful due to their efficient reflection and diffraction of visible light. In addition, due to their honeycomb lattice structure, these arrays can act as photonic band gap crystals in the visible frequency range. In this report, we present the initial exploration of the optical properties of such arrays. Here we show that these potential 2D photonic band gap crystal arrays might find very important applications in optoelectronics.

Ever since the first successful synthesis of well-aligned carbon nanotubes (CNTs) on substrates by plasma-enhanced chemical vapor deposition (PECVD),[1] numerous attempts have been reported on growth, characterization, and properties of aligned carbon nanotubes made by the same technique or its slight modification.[2−16] The catalyst used was either a thin film of Ni/Fe/Co made by magnetron sputtering[1−10] or dots made by electron beam (e-beam) lithography[11−15] or electrochemical deposition.[16] The arrays grown from either the thin film or from the dots by electrochemical deposition are inexpensive and can be of large area, but are nonperiodic. The arrays grown from dots made by e-beam lithography are periodic, but are limited to a very small area and are very expensive. It is clear that a self-assembly technique is needed to overcome these problems.

Here we report the development of such a self-assembly nanosphere lithography.[17] This technique utilizes the commercially available (Microparticles, GmbH) monodisperse suspensions of polystyrene nanospheres. We investigated nanospheres with diameters of 1, 0.5, 0.25, and 0.125 μm. First, a small amount of the suspension (4−6 μL) was applied onto the surface of a clean, large silicon wafer. Subsequently, the silicon wafer was immersed into the deionized water, and a highly ordered, large area monolayer of nanospheres formed on the water surface after proper modification of the surface tension with dodecylsodiumsulfate solution.[18] By draining the water, this defectless monolayer can be deposited on the surface of any sufficiently flat substrate. Figure 1a shows a monolayer of polystyrene spheres deposited on a 10 mm × 10 mm Si substrate. The uniform diffraction color in Figure 1b shows that this indeed is a highly ordered, essentially defectless monolayer. This is further confirmed by the fast Fourier transform (FFT) analysis (shown in Figure 1c).

The nanosphere arrays are subsequently used as a mask for deposition of the catalyst (Fe, Co, or Ni). Electron beam evaporation of Ni has been employed. After the deposition of Ni, the polysterene particles are chemically removed in toluene. Figure 2a shows the AFM image of the honeycomb pattern of Ni dots (of quasi triangular shape) after removal of the polystyrene spheres. These dots can be used directly, or after annealing (in a vacuum at 900 °C for 1 h to form arrays shown in Figures 2b and 2c) to grow aligned carbon nanotube arrays.[17]

Hot filament PECVD[1] was used to grow the aligned carbon naotube arrays. The details of the growth technique have been extensively reported.[1,2,11,12,16] Briefly, the substrates with the Ni dot arrays were first loaded into the bell jar chamber, then the chamber was pumped down to 10^{-6} Torr before the growth gases were introduced. Acetylene gas (C_2H_2) was used as the carbon source, whereas ammonia gas (NH_3) was

* Corresponding author. E-mail: renzh@bc.edu.
[†] Boston College.
[‡] Natick Soldier Center.
[§] Hahn-Meitner-Institute.
[||] NanoLab, Inc.
[⊥] University of Massachusetts.

10.1021/nl0258271 CCC: $25.00
Published on Web 11/19/2002

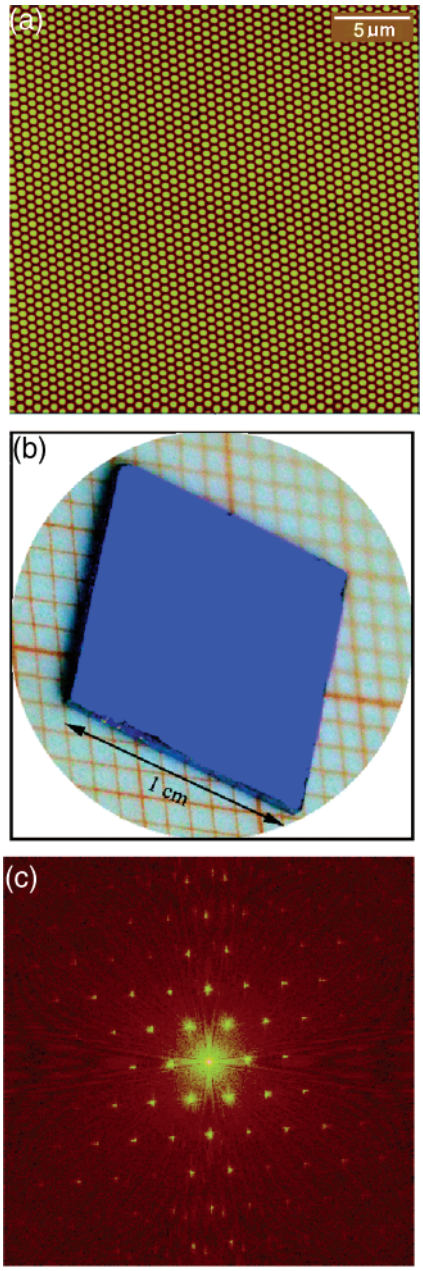

Figure 1. Highly ordered monolayer of polystyrene nanospheres (diameter 0.5 μm) on Si substrate made by the self-assembly nanosphere lithography. (a) AFM image of the closely packed hexagonal nanospheres, (b) single blue color of the area 10 × 10 mm^2, (c) FFT showing the high quality of the array.

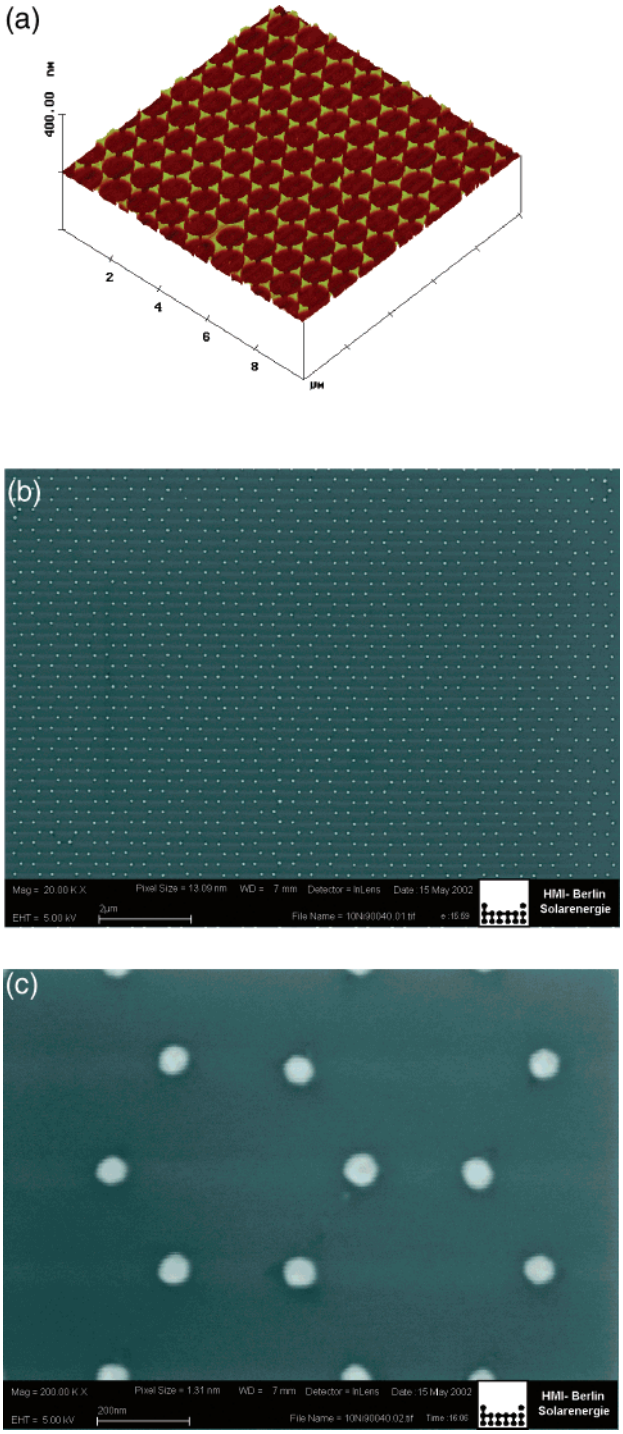

Figure 2. AFM and SEM images of the Ni dots made by nanosphere lithography. (a) AFM image of the Ni dots made from the nanospheres, low (b) and high (c) magnifications of the round Ni dots after annealing at 900 °C in vacuum for 1 h.

used as the plasma enhancer and growth promoter. After the chamber pressure reached about 5−20 Torr, a hot filament was powered up to provide heat to the substrate and to help in plasma generation. The plasma was maintained at about 600−800 V and 0.2−0.3 A. Growth takes usually 5−10 min depending on the carbon nanotube length requirement. Figures 3a and 3b show SEM images of the typical array at low and medium magnification, respectively. It is worth noting that the straightness of these nanotubes is not as good as that reported before.[1,11,12] The reason might be related to imperfections in the removal of polystyrene nanospheres from the substrate after Ni deposition or to the growth conditions themselves, but not to the catalyst patterning, since very straight nanotubes have been grown on the electron-beam patterned Ni dots before.[11,12] We are confident that the quality can and will be improved with better care of the polystyrene nanosphere removal and better control of the growth. The optical properties of these periodic arrays were studied thoroughly, and results are presented in the following sections.

After growth, the periodic arrays of aligned nanotubes appear colorful (see Figure 3c). This strong diffraction of

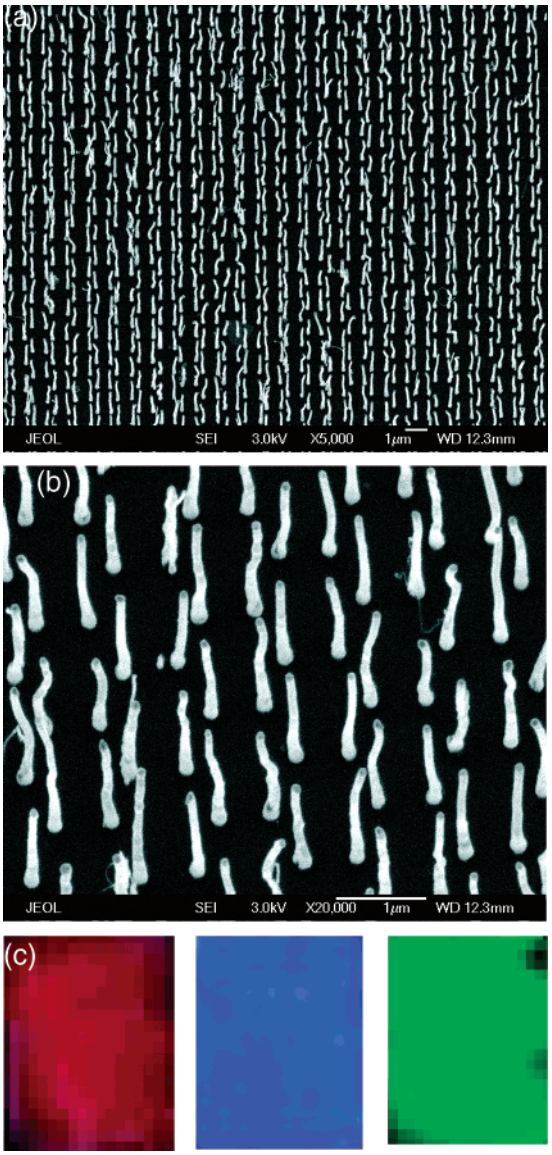

Figure 3. Low (a) and high (b) magnification SEM images of the highly ordered honeycomb array of aligned carbon nanotubes grown by PECVD, (c) bright diffraction colors of red, blue, and green.

visible light demonstrates the high metallicity of the nanotubes (low dielectric losses) and the high degree of ordering in the arrays.

The general theory of light diffraction can be used to show that such honeycomb arrays will lead to a triangular diffraction pattern. The honeycomb lattice is a hexagonal two-dimensional (2D) Bravais lattice with a basis (shown in Figure 4a).[19] The primitive translation vectors of the lattice are $a_1 = a(1, 0)$ and $a_2 = a(-1/2, \sqrt{3}/2)$. The basis vectors are $c_1 = 0$ and $c_2 = (a_1 + 2a_2)/3$. The corresponding reciprocal lattice in 2D is triangular (shown in Figure 4b).[19] The corresponding primitive reciprocal lattice vectors are $b_1 = s(\sqrt{3}/2, 1/2)$ and $b_2 = s(0, 1)$, where $s = 4\pi/a\sqrt{3}$. Also shown is the first Brillouin zone. In 3D, the reciprocal lattice is an array of parallel lines (G-lines), each perpendicular to the 2D reciprocal lattice, and each going through a reciprocal lattice point, given by the reciprocal lattice vector $\mathbf{G} = mb_1 + nb_2$.[20]

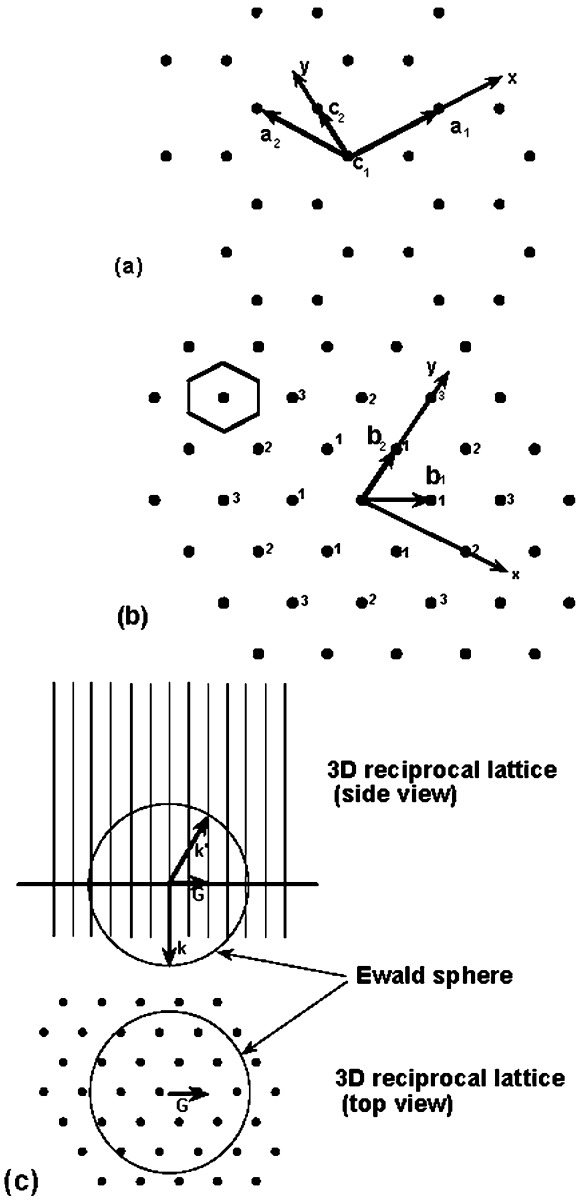

Figure 4. (a) The honeycomb lattice, (b) the 2D triangular reciprocal lattice of the honeycomb lattice, and (c) the 3D reciprocal lattice of the 2D honeycomb lattice.

The differential cross-section for light scattering $\zeta(q)$ is given by[19]

$$\zeta(q) \propto |U_\alpha(q)|^2 I(q) \tag{1}$$

where $U_\alpha(q)$ is the scatterer form factor, and $q = K' - K$ is the in-plane momentum transferred to the lattice in the scattering process. $K(K')$ is the in-plane component of the wave vector of the incident (scattered) wave. $I(q)$ is the structure factor given by

$$I(q) = \sum_G |\langle n_G \rangle|^2 \, \delta(q - G) + S(q) \tag{2}$$

where $S(q)$ is the Ursell function (a measure of the spatial

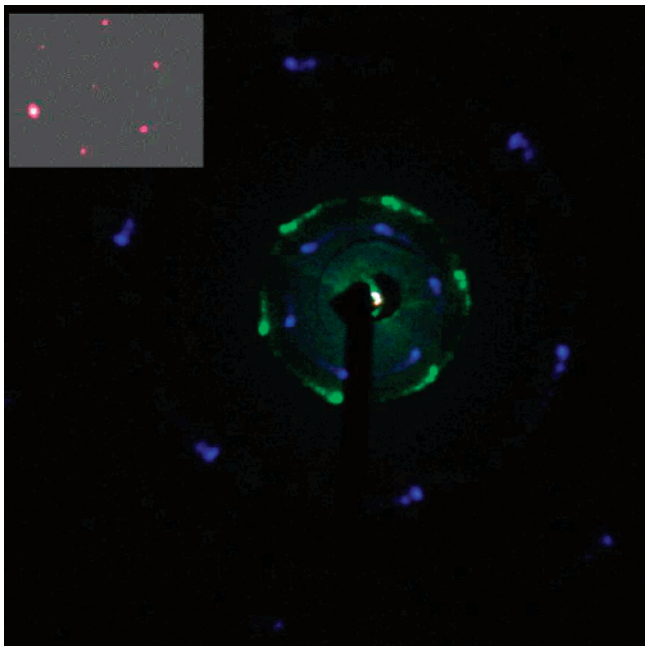

Figure 5. Diffraction pattern of light at different frequencies by the nanotube arrays shown in Figure 3 (inset: diffraction pattern of red color).

correlations of the local density fluctuations) and $\langle n_G \rangle$ is the ensemble average of the Fourier component (at G) of the charge density, which in the case of the honeycomb lattice of point scatterers is given by

$$|\langle n_G \rangle|^2 = |\sum_{i=1}^{2} \exp(-iGc_j)|^2 = 2\left\{1 + \cos\left[\frac{4\pi}{3}\left(\frac{m}{2} + n\right)\right]\right\} \quad (3)$$

For a defectless crystal, the Ursell function is zero and the scattering is governed by the Bragg diffraction, i.e., $\zeta(q)$ sharply peaked at $q = G$.

A plane wave incident normal to the lattice has its wave vector k, which has no in-plane component, i.e., $K = 0$. The problem here is very similar to that of the low energy electron diffraction (LEED).[20] Figure 4c shows that the diffraction pattern is just the projection of the reciprocal lattice onto a spherical screen (with its center on the sample), and therefore the diffraction pattern obtained from our honeycomb lattice should be a triangular lattice. From Figure 4c it is also obvious that only a limited number of diffraction spots (up to a given order) will occur for a given radius of the Ewald sphere and given parameters of the reciprocal lattice (only those lattice points which are encircled by the circumference of the Ewald sphere in Figure 4c project into the diffraction spots).

Figure 5 shows a diffraction pattern obtained from a nanotube array of Figure 3, with $a = 1\ \mu$m. The pattern was obtained by shining green (560 nm) and blue (454 nm) laser light perpendicular to the plane of the lattice. The projection was made onto an almost flat screen, which allowed for an observation of a large portion of the projected reciprocal space but caused a distortion of the triangular symmetry of the pattern. Apart from this, the pattern is highly rotationally symmetric (except for the third order blue diffraction spots), showing that our scatterers (nanotubes) are circularly symmetric in the plane. Note that there is a rather small hexatic distortion of the pattern, indicating presence of a possible formation of misaligned crystalline macro regions. There is also a small diffusive scattering (nonzero Ursell function) resulting from the fact that the nanotubes are not perfectly straight (see Figure 3). For perfectly straight nanotubes the diffraction spots would be points, and the green background around the central spot would disappear. The amount of the spot broadening can be estimated using the Debye−Waller factor and assuming that bent nanotubes can be viewed as effectively displaced from the lattice sites. We estimate from Figure 3 that the mean relative (to lattice constant) displacement of nanotubes is about 10%, and thus expect a similar degree of spot broadening relative to the spot distance, in agreement with Figure 5.

For this lattice

$$|G| = s\sqrt{\frac{3m^2}{4} + \left(\frac{m}{2} + n\right)^2} \quad (4)$$

For the first, second, and third order (see Figure 4c), we have $|G| = G_1 = s = 7.25\ \mu\text{m}^{-1}$, $|G| = G_2 = s\sqrt{3} = 12.5\ \mu\text{m}^{-1}$, $|G| = G_3 = 2s = 14.5\ \mu\text{m}^{-1}$, respectively. The radius of the Ewald sphere is $|k| = 11.2\ \mu\text{m}^{-1}$ for the green light and $13.8\ \mu\text{m}^{-1}$ for the blue light. This immediately implies that the green light should experience diffraction only of the first order, since only $G_1 < |k|$. Figure 5 shows that this indeed is the case. Since for the blue light $G_1 < G_2 < |k|$, only first- and second-order diffraction is expected for strictly normal incidence. Figure 5 shows that in addition to highly symmetric first- and second-order spots of the blue light, there are visible four third-order spots, asymmetrically distributed on the lower-right half of the diffractogram. These peaks result from the fact that the incoming light was not strictly normal to the plane, which shifts the Ewald sphere (by K) away from a reciprocal lattice point. Thus, in our case, a small in-plane component K, due to a slight tilt of the incoming wave with respect to the lattice normal, enabled the crossing of the Ewald sphere with the otherwise inaccessible G-line, and the third-order "forbidden" spots appeared. This way, by tilting the incoming beam, one can "walk" across the projected reciprocal lattice. We have confirmed that in this way the second-order "forbidden" spots of the green light can be also recovered.

There is also a specific dependency of the intensity of the spots on their order. If the scatterer lattice were without basis, $\langle n_G \rangle$ would be 1 and the structure factor $I(q)$ would consist of Bragg spots with equal intensity. The scattering cross-section would then reflect the usual behavior of the scatterer form factor and would consist of Bragg spots decaying uniformly with the order. This indeed is the case for the Fourier transform of the triangular lattice of PS spheres (see Figure 1c). Since the honeycomb lattice is a triangular lattice with a basis, $|\langle n_G \rangle|^2$ is given by eq 3 and is equal to 1 for the first and third order, but 4 for the second order. Therefore, even with the form factor decay, the second-order spots

should be brighter than the first, and of course much brighter than the third-order spots. This is again fully consistent with Figure 5, which shows precisely this behavior for the blue light diffraction. The inset in Figure 5 shows the diffraction pattern for a red light (680 nm), obtained at incidence of 45°. Note that there is an asymmetry of the spot intensity favoring the forward reflection. This reflects the fact that with increasing angle of incidence, the diffraction pattern must evolve into the in-plane scattering, which according to the Laue construction should consist of only one diffraction spot for a given incoming direction.

In addition to these straightforward diffraction effects, our arrays of nanotubes can act also as 2D photonic band gap crystals. It has been shown[21] that periodic arrays of structures having dielectric constants (ϵ_a) different from the environment (ϵ_b) not only act on propagating photons by enforcing the Bragg scattering as discussed above but also, in complete analogy to the electron propagation in atomic crystals, lead to the opening of energy (frequency) gaps at the Bragg reflection points, i.e., at the Brillouin zone boundaries. If such gaps occur at all propagation directions of the photon (or electron), an absolute gap exists in the photonic spectrum, which in the case of the photonic crystal leads to a total reflection of light in this frequency band. It has been shown[22,23] that a honeycomb array of rods, with a large dielectric constant, embedded in a material with a low dielectric constant, produces a photonic band structure with absolute gaps at low fillings. This was later confirmed by an experiment in the microwave frequency range[24] and very recently in the infrared frequency range,[25] in perfect agreement with the theory. It was also shown that a simple size scaling ($\omega \sim 1/a$) holds for the gaps, and therefore one can simply rescale the results of these papers to systems with different sizes, such as honeycomb arrays of nanotubes.

Even though our nanotubes have a dielectric constant that is different from that of the nanorods considered in refs 22−24, we can still directly employ results of these references to our arrays of nanotubes, after proper dielectric constant scaling. First we note that in the theory of refs 22−23, all the relative sizes of the gaps $\delta_i = |\Delta\omega_i/\omega_i|$ are approximately proportional to the Fourier components of the perturbation (dielectric constant inhomogeneity), which in turn, for a system with $\epsilon_a > \epsilon_b$, are proportional to $p = 1/\epsilon_b - 1/\epsilon_a$. Therefore, we find that $\delta_i \sim p$. Since this is the only dependency on ϵ_a and ϵ_b in the gap equations, the results for various gaps obtained in refs 22−23 can be simply scaled (by using p) to obtain corresponding results for systems with different dielectric constants. Using this, we immediately show that the honeycomb array of our nanotubes obtained by using nanospheres of diameter 0.5 μm should act as a 2D photonic band gap crystal with the gap at the radiation wavelength $\lambda \approx 0.5$ μm. Since our metallic nanotubes have $\epsilon_a < 0$ in the visible frequency range (their plasma frequency is at 6.5 eV); this yields $p > 1$, and therefore the gap size is expected to be $\delta_2 > 15\%$. Note that since the dielectric constant of nanotubes has also an imaginary part (losses), the gap does not imply a perfect reflection. The experimental effort to demonstrate the photonic band gap in our nanotube arrays is in progress. In view of ref 25, we feel confident that we can obtain photonic band gaps in the visible range. This would be very difficult to achieve using the fabrication method of ref 25. In addition, our method is very inexpensive and scalable. The imperfections in the nanotube straightness will tend to reduce the photonic band gap size, in full analogy to the gap reduction in the electronic crystals. The size of this reduction scales with the mean effective displacement (due to bending) of nanotubes from the lattice sites and is expected (as discussed above) to be about 10% for the array shown in Figure 3.

We note that the nanotubes can be coated for better control of the photonic crystal parameters. They can also be used as structural templates, to obtain nonmetallic photonic arrays, including nonmetallic 2D band gap crystals.

In conclusion, we report here a scalable inexpensive technique to fabricate large periodic arrays of carbon nanotubes. These arrays not only reflect and diffract light but can also have a photonic band gap in, or around, the visible frequency range. The precise frequency location and size of this gap can be controlled by the structural and material parameters of the arrays.

Acknowledgment. This work is supported partly by The U.S. Army Natick Soldier Systems Center under grants DAAD16-02-C-0037 and DAAD16-00-C-9227, partly by the DOE under grant DE-FG02-00ER45805, and partly by the NSF under grant ECS-0103012.

References

(1) Ren, Z. F.; Huang, Z. P.; Xu, J. W.; Wang, J. H.; Bush, P.; Siegal, M. P.; Provencio, P. N. *Science* **1998**, *282*, 1105.
(2) Huang, Z. P.; Xu, J. W.; Ren, Z. F.; Wang, J. H.; Siegal, M. P.; Provencio, P. N. *Appl. Phys. Lett.* **1998**, *73*, 3845.
(3) Fan, S. S.; Chapline, M. G.; Franklin, N. R.; Tombler, T. W.; Cassell, A. M.; Dai, H. J. *Science* **1999**, *283*, 512.
(4) Choi, Y. C.; Shin, Y. M.; Lee, Y. H.; Lee, B. S.; Park, G. S.; Choi, W. B.; Lee, N. S.; Kim, J. M. *Appl. Phys. Lett*. **2000**, *76*, 2367.
(5) Merkulov, V. I.; Lowndes, D. H.; Wei, Y. Y.; Eres, G.; Voelkl, E. *Appl. Phys. Lett*. **2000**, *76*, 3555.
(6) Bower, C.; Zhu, W.; Jin, S. H.; Zhou, O. *Appl. Phys. Lett*. **2000**, *77*, 830.
(7) Lee, C. J.; Park, J.; Kang, S. Y.; Lee, J. H. *Chem. Phys. Lett*. **2000**, *326*, 175.
(8) Han, J.; Yang, W. S.; Yoo, J. B.; Park, C. Y. *J. Appl. Phys*. **2000**, *88*, 7363.
(9) Ho, G. W.; Wee, A. T. S.; Lin, J.; Tjiu, W. C. *Thin Solid Films* **2001**, *388*, 73.
(10) Hayashi, Y.; Negishi, T.; Nishino, S. *J. Vac. Sci. Technol. A* **2001**, *19*, 1796.
(11) Ren, Z. F.; Huang, Z. P.; Wang, D. Z.; Wen, J. G.; Xu, J. W.; Wang, J. H.; Calvet, L. E.; Chen, J.; Klemic, J. F.; Reed, M. A. *Appl. Phys. Lett*. **1999**, *75*, 1086.
(12) Wen, J. G.; Huang, Z. P.; Wang, D. Z.; Chen, J. H.; Yang, S. X.; Ren, Z. F.; Wang, J. H.; Calvet, L. E.; Chen, J.; Klemic, J. F.; Reed, M. A. *J. Mater. Res.* **2001**, *16*, 3246.
(13) Wei, Y. Y.; Eres, G.; Merkulov, V. I.; Lowndes, D. H. *Appl. Phys. Lett*. **2001**, *78*, 1394.
(14) Teo, K. B. K.; Chhowalla, M.; Amaratunga, G. A. J.; Milne, W. I.; Hasko, D. G.; Pirio, G.; Legagneux, P.; Wyczisk, F.; Pribat, D. *Appl. Phys. Lett*. **2001**, *79*, 1534.
(15) Chhowalla, M.; Teo, K. B. K.; Ducati, C.; Rupesinghe, N. L.; Amaratunga, G. A. J.; Ferrari, A. C.; Roy, D.; Robertson, J.; Milne, W. I. *J. Appl. Phys*. **2001**, *90*, 5308.
(16) Tu, Y.; Huang, Z. P.; Wang, D. Z.; Wen, J. G.; Ren, Z. F. *Appl. Phys. Lett*. **2002**, *80*, 4018.
(17) Huang, Z. P.; Rybczynski, J.; Giersig, M.; Kempa, K.; Wang, D. Z.; Carnahan, D. L.; Wen, J. G.; Sennett, M.; Ren, Z. F. *Appl. Phys. Lett*., submitted.

(18) Carnahan, D. L., patent pending.
(19) Chaikin P. M.; Lubensky, T. C. *Principles of condensed matter physics*; Cambridge University Press: Cambridge, 2000.
(20) Murr, L. E. *Electron optical applications in material science*; McGraw-Hill: New York, 1970.
(21) Yablonovitch, E. *Phys. Rev. Lett*. **1987**, *58*, 2059.
(22) Cassagne, D.; Jouanin, C.; Bertho, D. *Phys. Rev. B* **1995**, *52*, R2217.
(23) Cassagne, D.; Jouanin, C.; Bertho, D. *Phys. Rev. B* **1996**, *53*, 7134.
(24) Gadot, F.; Chelnokov, A.; Lustrac, A. D.; Crozat, P.; Lourtioz, J. M.; Cassagne, D.; Jouanin, C. *Appl. Phys. Lett*. **1997**, *71*, 1780.
(25) Ye, J. Y.; Mizeikis, V.; Xu, Y.; Matsuo, S.; Misawa, H. *Opt. Commun.* **2002**, *211*, 205.

NL0258271